Chemical Engineering Science: X 3 (2019) 100032

Contents lists available at ScienceDirect

Chemical Engineering Science: X

journal homepage: www.elsevier.com/locate/cesx

Kinetics of CO_2 absorption into aqueous solutions of 3-dimethylamino-1-propanol and 1-(2-hydroxyethyl)pyrrolidine in the blend with 3-(methylamino)propylamine

Ida M. Bernhardsen, Hanna K. Knuutila *

Department of Chemical Engineering, Norwegian University of Science and Technology (NTNU), NO-7491 Trondheim, Norway

ARTICLE INFO

Article history:
Received 11 February 2019
Received in revised form 29 May 2019
Accepted 14 July 2019

Keywords:
Chemical absorption
Amine blends
Kinetics
Solubility

ABSTRACT

The kinetics of CO_2 absorption into unloaded aqueous solutions of 3-dimethylamino-1-propanol (3DMA1P) and 1-(2-hydroxyethyl)pyrrolidine (1-(2HE)PRLD) blended with 3-(methylamino) propylamine (MAPA) were studied in the temperature range of 29–63 °C using a string of discs contactor. In addition, density and viscosity of the blended amines were measured in the temperature range of 25–80 °C, and N_2O solubility was measured in the temperature range of 30–90 °C. The obtained results were compared with blends of 2-(diethylamino)ethanol (DEEA) and MAPA.

The present study indicated that the blended amines, with varying solvent concentration, obtained comparable values for the overall mass transfer coefficient due to competing effects between solubility, diffusivity and reaction kinetics. The solubility of CO_2 was higher in DEEA/MAPA than in the other blended amines, while the calculated values for the pseudo-first order kinetic constant were higher for the 3DMA1P/MAPA and 1-(2HE)PRLD/MAPA solutions than for the DEEA/MAPA solution. The pseudo-first order kinetic constants were correlated to the direct mechanism with reasonable accuracy. The contribution of the tertiary amine as a proton receiver for the MAPA-CO_2 reaction represented between 53 and 70% of the pseudo-first order kinetic constant.

1. Introduction

Carbon capture and storage (CCS) is an important mitigation option to reduce anthropogenic CO_2 emission. The leading technology is amine-based chemical absorption, which has been used for decades to remove impurities in natural gas and other process gas streams. However, as a climate measure, it has not yet reached widespread implementation in the industry mainly due to the high-energy requirement for solvent regeneration, and high capital and operating costs (Steeneveldt et al., 2006). The development of new solvents with improved CO_2 capture performance is one of the strategies to minimise the drawbacks associated with the chemical absorption process. Especially, a great deal of research has been undertaken to study blended amine solvents (Du et al., 2016; Li et al., 2013; Sodiq et al., 2018). Blended amines have the potential of retaining much of the reactivity of the primary/secondary amines and at the same time provide an energy penalty lower than the benchmark solvent 30 wt% monoethanolamine (MEA) (Idem et al., 2006).

The present work focuses on the CO_2 reaction kinetics into blended amine solvents to evaluate their potential for CO_2 capture. The solvents reaction kinetics are important to study as the absorption rate is related to the height of the absorption column, and an improvement in absorption rate may result in a more affordable absorption column. The solvents studied in this work were blends of 3-dimethylamino-1-propanol (3DMA1P)/3-(methylamino)propylamine (MAPA) and 1-(2-hydroxyethyl)pyrrolidine (1-(2HE)PRLD)/MAPA. The diamine MAPA contains both a primary and a secondary amine group and has previously been used in a blend with for example 2-(diethylamino)ethanol (DEEA) (Pinto et al., 2014) and dimethylethanolamine (DMEA) (Brúder et al., 2012) with promising results. As a single amine, Monteiro et al. (2014) reported that the pseudo-first order kinetic constant (k_{obs}) for 1 M MAPA at 25 °C was around 15 times faster than 1 M MEA and twice as fast as 1 M PZ.

In this work, the initial reaction rate of CO_2 into the blended amines was studied in the temperature range of 29–63 °C using a string of discs contactor, and under conditions fulfilling the pseudo-first order assumption. To evaluate the CO_2 absorption rate, density, viscosity and N_2O solubility of the blended amines were also measured. In addition, to give a comprehensive

* Corresponding author.
E-mail address: hanna.knuutila@ntnu.no (H.K. Knuutila).

https://doi.org/10.1016/j.cesx.2019.100032
2590-1400/

Nomenclature

c	concentration, kmol m^{-3}, mol m^{-3}
D	diffusivity, m^2 s^{-1}
E	enhancement factor
E_∞	infinite enhancement factor
H	Henry 's law constant, kPa m^3 mol^{-1}
Ha	Hatta number
k	kinetic constant, m^6 mol^{-2} s^{-1}
k_g	gas-side mass transfer coefficient, m s^{-1}
k_l^0	liquid-side mass transfer coefficient without reaction, m s^{-1}
k_{obs}	pseudo-first order kinetic constant, s^{-1}
K_{ov}	overall mass transfer coefficient, mol m^{-2} kPa^{-1} s^{-1}
N	absorption flux, mol m^{-2} s^{-1}
n_{N2O}	mole of N_2O in the liquid phase
p	partial pressure, kPa
P	total pressure, kPa
r	reaction rate constant, mol m^{-2} s^{-1}
T	temperature, °C
v	stoichiometric coefficient
V	volume, m^3
X	any base present in the solution
y	mole fraction

Greek symbols

Γ	wetting rate, kg m^{-1} s^{-1}
μ	viscosity, mPa s
ν	velocity, m s^{-1}
ρ	density, g cm^{-3}

Subscripts

0	initial state
b	bulk
i	interface
L	liquid phase

Superscripts

g	gas phase
LM	logarithmic mean

Abbreviations

AARD	average absolute relative deviation
DEEA	2-(diethylamino)ethanol
FS	full scale
MAPA	3-(methylamino)propylamine
MEA	monoethanolamine
3DMA1P	3-dimethylamino-1-propanol
1-(2HE)PRLD	1-(2-hydroxyethyl)pyrrolidine

understanding of systems promoted by MAPA, experimental and estimated values were compared to blends of DEEA/MAPA reported by Monteiro et al. (2015) and the 1 M MAPA solution reported by Monteiro et al. (2014).

2. Chemical reactions

The absorption of CO_2 into aqueous blended amine solutions occur through a set of acid-base reactions in the liquid phase forming mainly amine carbamate ($RNCOO^-$), (bi)carbonate (HCO_3^-/CO_3^{2-}) and protonated amine. The reactions of CO_2 in aqueous solution of primary, secondary or tertiary amines have been extensively studied in the literature (Blauwhoff et al., 1984; Caplow, 1968; Donaldson and Nguyen, 1980) while the specific reaction pathway in blended amines has not yet been fully understood. This is mainly due to potential interaction reactions between the amines in the solution, the influence of the amine composition on the reaction pathway and due to increased complexity when mixing amine groups reacting differently with CO_2. Recently, Perinu et al. (2019) studied the reactions occurring in the 3 M DEEA + 1 M MAPA solution in the CO_2 loading range of 0.04–0.77 mol_{CO2}/mol_{amine}. The study indicated that at the lowest CO_2 loading, the main reactions occurring were the formation of primary (p) and secondary(s) MAPA carbamate ($MAPACOO^-_{(p)/(s)}$) in which $MAPACOO^-{}_{(p)}$ was present in a larger amount. At this CO_2 loading, MAPA dicarbamate was present in a negligible amount, while (bi)carbonate was not detected before a CO_2 loading of 0.14 mol_{CO2}/mol_{amine}. In addition, Bernhardsen et al. (2019b) showed that the speciation data in CO_2 loaded solutions of DEEA/MAPA were comparable to the speciation data detected in CO_2 loaded solutions of 3DMA1P/MAPA and 1-(2HE)PRLD/MAPA. The similar speciation data indicated that 3DMA1P and 1-(2HE)PRLD affected MAPA reactions and CO_2 hydration similarly as DEEA. Thus, based on the speciation studies, the following reaction can be considered as the dominant reaction between CO_2 and the aqueous blended amine solution at zero loading:

$$MAPA + CO_2 + X \leftrightarrows MAPACOO^-{}_{(p)/(s)} + XH^+ \tag{1}$$

where X is any base present in the solution acting as counter-ion, i.e. R_3N, H_2O and MAPA.

The mechanism for this reaction can be described using the direct mechanism, previously used to describe DEEA/MAPA systems (Monteiro et al., 2015), as given in Eq. (2).

$$r_{CO_2} = \left(k_{MAPA}c_{MAPA} + k_{H_2O}c_{H_2O} + k_{R_3N}c_{R_3N}\right)c_{MAPA}c_{CO_2} \tag{2}$$

3. Mass transfer

The mass transfer of CO_2 from the bulk gas phase to the bulk liquid phase, accompanied by chemical reaction, can be interpreted using the two-film theory. The film theory (Danckwerts, 1970) assumes that all resistance to mass transfer is restricted to two stagnant films near the gas-liquid interface. Under steady state conditions, the flux of CO_2 through the films is constant as given in Eq. (3).

$$N_{CO_2} = k_g\left(p_{CO_2,b} - p_{CO_2,i}\right) = Ek_l^0\left(c_{CO_2,i} - c_{CO_2,b}\right) \tag{3}$$

At the interface, the equilibrium is governed by Henry's law (Eq. (4)) and by combining Eqs. (3) and (4), the overall mass transfer coefficient, K_{ov}, based on the driving force for the gas phase is expressed as given in Eq. (5).

$$H_{CO_2} = \frac{p_{CO_2,i}}{c_{CO_2,i}} \tag{4}$$

$$K_{OV} = \frac{1}{\frac{1}{k_g} + \frac{H_{CO_2}}{Ek_l^0}} \tag{5}$$

Further, for fast reacting systems, operation in the pseudo first order regime can be assumed if the reactions are irreversible and the access of absorbent is large. Then, Eq. (2) can be considered first order with respect to CO_2 (Eq. (6)) and the pseudo-first order kinetic constant (k_{obs}) is expressed as given in Eq. (7).

$$r_{CO_2} = k_{obs} c_{CO_2} \tag{6}$$

$$k_{obs} = \left(k_{MAPA} c_{MAPA} + k_{H_2O} c_{H_2O} + k_{R_3N} c_{R_3N}\right) c_{MAPA} \tag{7}$$

The requirements for the use of the pseudo-first order assumption is that the following two conditions are fulfilled (Haubrock et al., 2007):

$$Ha > 3 \tag{8}$$

$$\frac{E_\infty}{Ha} > 5 \tag{9}$$

The Hatta number, Ha, is defined as given in Eq. (10) and the infinite enhancement factor, E_∞, is expressed as given in Eq. (11) when it is defined from the film model.

$$Ha = \frac{\sqrt{k_{obs} D_{CO_2,solution}}}{k_L^0} \tag{10}$$

$$E_\infty = 1 + \frac{D_{amine,solution} c_{amine}}{\nu D_{CO_2,solution} c_{CO_2,i}} \tag{11}$$

Given that Eq. (1) takes place under conditions fulfilling the pseudo-first order assumption (Eqs. (8) and (9)), the enhancement factor, E, in Eq. (5) can be set equal to the Hatta number (Eq. (10)), and the pseudo-first order kinetic constant (k_{obs}) can be calculated as given in Eq. (12).

$$k_{obs} = \frac{H_{CO_2}^2}{\left(\frac{1}{K_{OV}} - \frac{1}{k_g}\right)^2 D_{CO_2,solution}} \tag{12}$$

4. Physiochemical properties

To calculate the pseudo-first order kinetic constant, information about the systems viscosity, solubility and diffusivity are required. The diffusivity of CO_2 into the amine solution, $D_{CO_2,solution}$, was calculated according to the modified Stokes-Einstein relation proposed by Versteeg and Van Swaaij (1988) (Eq. (13)) in which the diffusivity of CO_2 in pure water, $D_{CO_2,water}$, is given by Eq. (14) and the viscosity of pure water, μ_{water}, was estimated from the correlation provided by Bingham and Jackson (1917) (Eq. (15)). The viscosity was expressed as fluidity which is the reciprocal of viscosity. The viscosity of the amine solutions was measured experimentally (see Section 5.2.1).

$$D_{CO_2,solution} = D_{CO_2,\,water}\left(\frac{\mu_{water}}{\mu_{solution}}\right)^{0.8} \tag{13}$$

$$D_{CO_2,\,water} = 2.35 \times 10^{-6} \exp\left(\frac{-2119}{T}\right) \tag{14}$$

$$\mu_{water} = \frac{100}{2.1482\left[(T - 281.585) + \sqrt{8078.4 + (T - 281.585)^2}\right] - 120} \tag{15}$$

The N_2O-CO_2 analogy which was first proposed by Clarke (1964) was used to estimate the Henry's law constant for CO_2 in the amine solution, $H_{CO_2,solution}$:

$$H_{CO_2,solution} = H_{N_2O,\,solution}\left(\frac{H_{CO_2,water}}{H_{N_2O,water}}\right) \tag{16}$$

The Henry's law constant for CO_2 in pure water, $H_{CO_2,water}$, was estimated using the correlation provided by Carroll et al. (1991) (Eq. (17)), and the Henry's law constant for N_2O in pure water, $H_{N_2O,water}$, was estimated from the correlation provided by Penttilä et al. (2011) (Eq. (18)). The Henrys law constant for N_2O into the amine solution, $H_{N_2O,solution}$, was experimentally determined (see Section 5.2.2).

$$H_{CO_2,\,water} = \exp\left(145.369 + \frac{-8172.355}{T} - 19.303 \ln T\right) \tag{17}$$

$$H_{N_2O,\,water} = \exp\left(158.245 + \frac{-9048.596}{T} - 20.860 \ln T - 0.00252T\right) \tag{18}$$

5. Materials and experimental methods

5.1. Materials

Chemicals used in this work (Table 1) were used as received with no further purification. The amine solutions were prepared by weighing the required amount of chemical using MS6002S Mettler Toledo balance (accuracy ± 0.01 g) and diluting with deionised water to the desired concentration. The aqueous solutions studied in this work were: 2 M 3DMA1P + 1 M MAPA, 3 M 3DMA1P + 1 M MAPA, 4 M 3DMA1P + 1 M MAPA and 3 M 1-(2HE)PRLD + 1 M MAPA. The molecular structure of the amines studied is shown in Fig. 1.

5.2. Experimental methods

5.2.1. Viscosity and density measurements

Viscosity and density were measured using the Anton Paar Modulyzer multiparameter analysis system consisting of an Anton Paar Lovis 2000 ME rolling-ball viscometer and an Anton Paar DMA 4500 M density meter (Evjen et al., 2019). The measurements were conducted in the temperature range of 25–80 °C. For each sample, two viscosity and density measurements were carried out and the average value was reported.

5.2.2. Solubility apparatus

The physical solubility of N_2O in aqueous amine solutions was measured using the apparatus described in Gondal et al. (2015a). The apparatus consisted of a 1L jacketed Büchi glass reactor, a 1L gas holding vessel and a condenser placed at the top of the reactor. The pressure in the reactor and in the gas holding vessel was recorded by the pressure transmitter PTX5072 with a pressure range of 0–6 bar (FS ± 0.04%). In addition, a second pressure transmitter (PTX7517-1) was mounted to the reactor to cover the pressure range of 0–2 bar (FS ± 0.1%). Gas and liquid temperature were recorded by Pt-100 thermocouples (uncertainty ± 0.1 °C).

For each experiment, the reactor was evacuated, fed with a known amount of solution (around 450 g) and evacuated again at room temperature (25 °C) for around one minute. To minimise the risk of solvent loss during evacuation, the temperature of the condenser was maintained at 4 °C. After degassing, the solution was stirred at 500 rpm and heated to 30, 40, 50, 60, 70, 80 and 90 °C. Equilibrium was established at each temperature and a temperature-pressure profile before addition of N_2O was obtained. The establishment of equilibrium was automatically determined according to a set of criteria. The criteria were that the variance in reactor pressure and liquid/gas temperature, in a period of one minute, were less than 0.5 kPa, 0.015 °C and 0.025 °C, respectively, and that the difference between gas and liquid temperature was less than 0.1 °C. These conditions were typically fulfilled within 3–4 hrs.

After equilibrium was established at 90 °C, N_2O was added from the gas holding vessel to the reactor and the system was again left

Table 1
Chemicals used in this work.

Chemical	CAS	Molar mass [g/mol]	Purity	Supplier
3-(Methylamino)propylamine (MAPA)	6291-84-5	88.15	≥97%	Sigma-Aldrich
3-Dimethylamino-1-propanol (3DMA1P)	3179-63-3	103.16	99%	Acros organics
1-(2-Hydroxyethyl)pyrrolidine (1-(2HE)PRLD)	2955-88-6	115.17	97%	Alfa Aesar
2-(Diethylamino)ethanol (DEEA)	100-37-8	117.19	≥99.5	Sigma-Aldrich
Carbon dioxide (CO_2)	124-38-9	44.01	99.999%	AGA
Nitrogen (N_2)	7727-37-9	28.01	99.998%	AGA
Nitrogen oxide (N_2O)	10024-97-2	44.01	99.999%	AGA

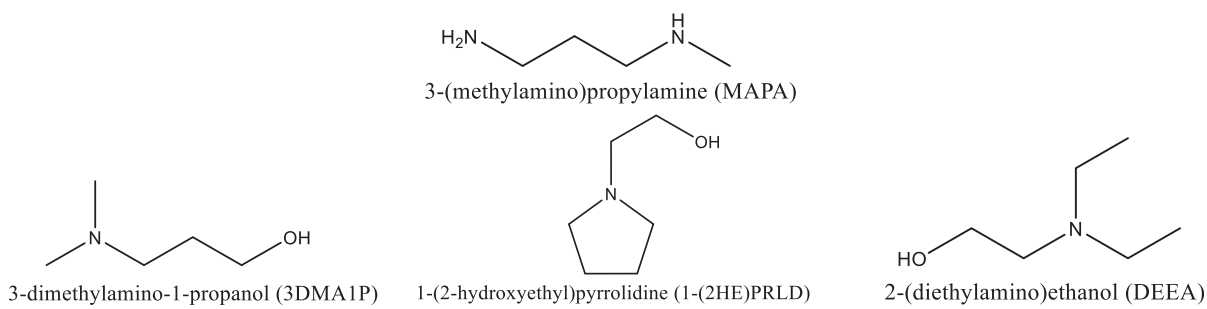

Fig. 1. Molecular structure of the amines studied in this work.

to equilibrate. Then, the temperature was gradually decreased, and equilibrium was established at each temperature. This resulted in a temperature-pressure profile after the addition of N_2O.

The data obtained from this experiment allowed for the calculation of the Henry's law constant, H_{N_2O}, (Eq. (19)).

$$H_{N_2O} = \frac{p_{N_2O}}{c_{N_2O}} \tag{19}$$

In the equation, P_{N_2O} is the partial pressure of N_2O and c_{N_2O} is the concentration of N_2O in the amine solution at a given temperature. P_{N_2O} was calculated as the difference between the total pressure in the reactor after addition of N_2O, $P_{\text{after addition of } N_2O}$, and the total pressure in the reactor before the addition of N_2O, $P_{\text{before addition of } N_2O}$, (Eq. (20)).

$$p_{N_2O} = P_{\text{after addition of } N_2O} - P_{\text{before addition of } N_2O} \tag{20}$$

c_{N_2O} was calculated as given in Eq. (21) where the amount of N_2O added from the gas holding vessel, $n_{N_2O}^{added}$, and present in the gas phase of the reactor, $n_{N_2O}^{g}$, was calculated using the Peng-Robinson equation of state (Peng and Robinson, 1976).

$$c_{N_2O} = \frac{n_{N_2O}^{added} - n_{N_2O}^{g}}{V_L} \tag{21}$$

5.2.3. String of discs contactor apparatus

The CO_2 absorption rate of unloaded amine solutions was measured using the string of discs contactor illustrated in Fig. 2. The apparatus, previously explained by Gondal et al. (2015b), is placed in a heating chamber and consist of a glass column with 43 discs. Each disc has a diameter of 1.5 cm and a thickness of 4 mm. This gives a column height of 64.5 cm and a total mass transfer area of 0.0219 m^2. The apparatus is designed for atmospheric pressures and temperatures up to 70 °C.

During operation, the inlet gas composition, containing N_2 and CO_2, was set by a mass flow controller and, with a gas flow rate of around 3 m^3/hr, it was counter-currently contacted with the falling amine solution with a liquid rate of around 60 mL/min. At this liquid rate, a ripple-free and uniform film covered the surface of the discs. The inlet and outlet temperatures of the liquid and gas phase were registered by k-type thermocouples and the pressure was measured by a DP cell from Druck. The outlet CO_2 gas concentration was monitored by an IR CO_2 analyser and to avoid water condensation in the analyser, the gas was first cooled to around 10–15 °C before it was passed to the analyser. The IR analyser was calibrated before and after the experiment, and both calibrations were used in the calculation.

For each amine solution, the CO_2 absorption flux was measured for five different temperatures in the range of 29–63 °C. For each temperature, around 5 L of solution was pumped through the system and re-used for the next temperatures. The temperature and CO_2 concentration were recorded every 10 s and when stable conditions were maintained for at least 5 min (by visual inspection), the experiment was terminated. After each temperature, a liquid sample was taken for CO_2 and amine analysis to ensure that the experiments were operated with sufficient CO_2 driving force and to ensure that the amine concentration was not depleted by the reaction. The CO_2 concentration was determined by total inorganic carbon (TIC) analyses using TOC-L provided by Shimadzu and the amine content was determined by titrating with 0.2 N H_2SO_4 (Ma'mun et al., 2006). In all samples, the analysed CO_2 content was low (i.e. in the range of 0.004 to 0.025 mol_{CO2}/mol_{amine}) and therefore assumed to be in an acceptable range with respect to the used driving force of 0.18–0.24 kPa CO_2.

From the logged experimental data, the overall mass transfer coefficient, K_{ov}, was calculated as the ratio between the CO_2 absorption flux, N_{CO_2}, and the driving force, $\Delta P_{CO_2}^{LM}$, (Eq. (22)).

$$K_{OV} = \frac{N_{CO_2}}{\Delta p_{CO_2}^{LM}} \tag{22}$$

N_{CO_2} was calculated from a mass balance as given in Eq. (23). The inlet flux of CO_2, $N_{CO_2,in}$, and N_2, $N_{N_2,in}$, respectively, was given directly from the mass flow controller. The outlet CO_2 flux, $N_{CO_2,out}$, was calculated using Eq. (24) where $N_{N_2,out} = N_{N_2,in}$ and the CO_2 mole fraction of the dried gas, y_{CO_2}, was as read from the IR analyser.

$$N_{CO_2} = N_{CO_2,in} - N_{CO_2,out} \tag{23}$$

$$N_{CO_2,out} = N_{N_2,out} \frac{y_{CO_2,out}}{\left(1 - y_{CO_2,out}\right)} \tag{24}$$

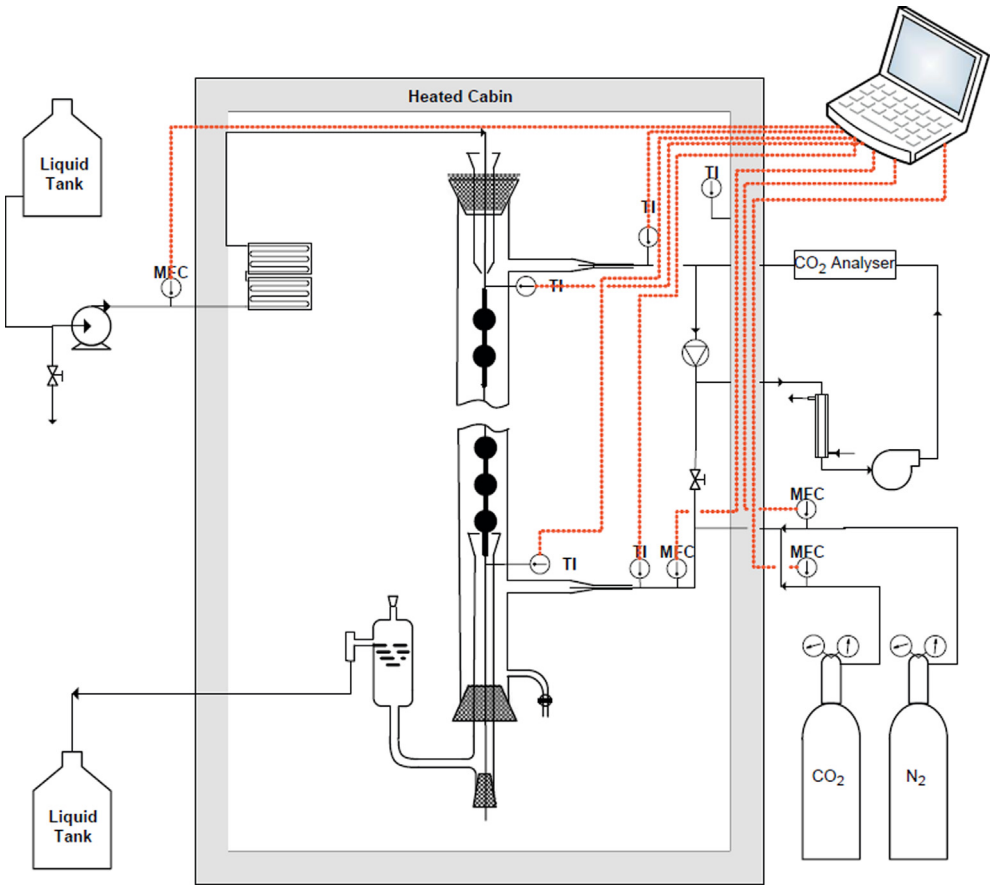

Fig. 2. Experimental set-up of the string of discs contactor. The figure is retrieved from Hartono et al. (2009).

$\Delta P_{CO_2}^{LM}$, was determined as the log mean average of the inlet and outlet CO_2 partial pressure, $p_{CO_2,in}$, and $p_{CO_2,out}$, respectively (Eq. (25)).

$$\Delta p_{CO_2}^{LM} = \frac{p_{CO_2,in} - p_{CO_2,out}}{\ln\left(\frac{p_{CO_2,in}}{p_{CO_2,out}}\right)} \tag{25}$$

For the string of discs contactor used in this work, the correlation for the liquid film mass transfer coefficient without chemical reaction, k_l^0, is given by Eq. (26) (Hartono et al., 2009), and the correlation for the gas film mass transfer coefficient, k_g, is given by Eq. (27) (Ma'mun et al., 2007).

$$\left(\frac{k_l^0}{D}\right) = 17.92\left(\frac{4\Gamma}{\mu}\right)^{1.0}\left(\frac{\mu}{\rho D}\right)^{0.5} \tag{26}$$

$$\left(\frac{k_g d}{D}\right) = 0.12\left(\frac{\rho \upsilon d}{\mu}\right)^{0.79}\left(\frac{\mu}{\rho D}\right)^{0.44} \tag{27}$$

In addition, the solvents vapour pressure was calculated using Raoult's law in which the pure components vapour pressure was estimated using Riedel or Antoine equations (Table 2).

6. Results and discussion

6.1. Validation of the experimental set-up

The viscosity and the density for the 4 M 3DMA1P + 1 M MAPA and 3 M 1-(2HE)PRLD + 1 M MAPA solutions were measured twice, and the repeatability of the viscosity and density measurement was 1.3% and $\pm 2\cdot 10^{-4}$ g/cm^3, respectively. The uncertainty of the viscosity and density measurement was, as reported in Evjen et al. (2019), 0.04 mPa·s and $2\cdot 10^{-3}$ g cm^{-3}, respectively.

The solubility apparatus was validated by measuring the solubility for CO_2 and N_2O into pure water and comparing to the correlation provided by Carroll et al. (1991) and Penttilä et al. (2011), respectively (Fig. 3, Appendix A). The average absolute relative deviation (AARD) between measured values and the literature was 1.5% for CO_2 and 1.3% for N_2O. The experiments were repeated twice, and on average, the repeatability was within 0.7%.

The string of discs contactor apparatus was validated by measuring the reaction kinetics of CO_2 into 30 wt% MEA in the temperature range of 28–61 °C. The AARD between the measured K_{ov} and the K_{ov} reported by Luo et al. (2015) was 9.1%, and the repeatability was on average 3.6%. The experimental data for 30 wt% MEA is reported in Bernhardsen et al. (2019a), but the data reported in this paper was run by the same operator and in the same period.

6.2. Evaluating the pseudo-first order assumption

The assumption of pseudo-first order was evaluated by considering the two conditions given in Eqs. (8) and (9). The Hatta number was calculated from Eq. (10) and is given in Appendix B.

First, as the Hatta number was at all time higher than 3, the condition given in Eq. (8) was fulfilled. Then, for the condition given in Eq. (9), the infinite enhancement factor, E_∞, was set equal to 5 times the value of the Hatta number and the lowest acceptable diffusivity coefficient of the amine in the aqueous amine solution, $D_{amine,\ solution}$, was calculated from Eq. (11). The $D_{amine,\ solution}$ for the solvents studied in this work is not known so this exercise also

Table 2
Parameters (A, B, C, D, E) for the Riedel and the Antoine equation.

	A	B	C	D	E	equation	Ref.
H_2O	73.649	−7258.2	−7.3037	$4.1653 \cdot 10^{-6}$	2	Riedel[a]	Perry et al. (1997)
MAPA	14.86	3530.43	−67.82			Antoine[b]	Hartono et al. (2013)
3DMA1P	10.169	−2065.352	−34.122			Antoine[c]	Bernhardsen et al. (2019b)
1-(2HE)PRLD	11.260	−2944.532	16.249			Antoine[c]	Bernhardsen et al. (2019b)

[a] $\ln(P_i^{sat}/Pa) = A + \frac{B}{T/K} + C\ln(T/K) + D(T/K)^E$.
[b] $\ln(P_i^{sat}/kPa) = A - \frac{B}{C + T/K}$.
[c] $\log_{10}(P_i^{sat}/Pa) = A + \frac{B}{T/K + C}$.

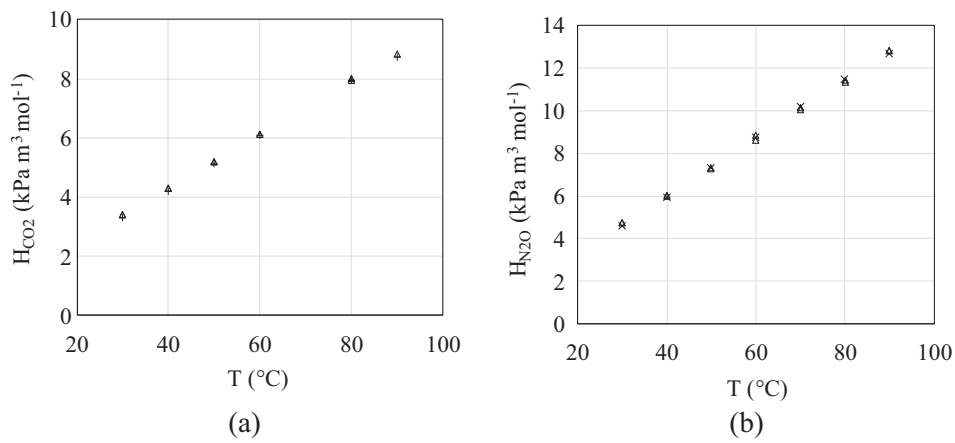

Fig. 3. Henry's law constant for (a) CO_2 in water and (b) N_2O in water. (Δ) this work; (+) Carroll et al. (1991); (×) Penttilä et al. (2011).

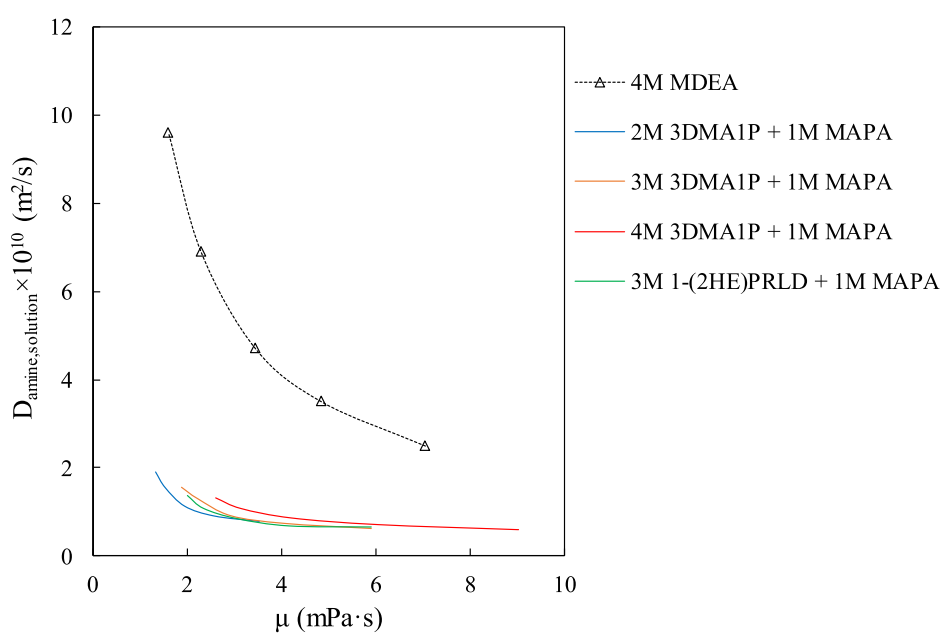

Fig. 4. The diffusivity coefficient of the amine in the aqueous amine solution, $D_{amine,solution}$, as a function of the solution viscosity, μ. (Δ) Snijder et al. (1993); coloured lines, lowest acceptable $D_{amine,solution}$ as calculated from Eq. (11).

studies how sensitive the pseudo-first order assumption is for the choice of $D_{amine,\ solution}$. Often, in the literature, $D_{amine,\ solution}$ is assumed similar to the $D_{amine,\ solution}$ measured for another amine. The lowest acceptable $D_{amine,\ solution}$ is shown in Fig. 4 and is compared to the diffusivity coefficient of 4 M MDEA in the MDEA solution, $D_{MDEA,\ solution}$, experimentally determined by Snijder et al. (1993) in the temperature range 25–75 °C. The comparison shows that the lowest acceptable $D_{amine,\ solution}$ ranges from 4 to 6 times lower than $D_{MDEA,\ solution}$. This indicates that the pseudo-first order assumption made in this work is valid as long as the $D_{amine,\ solution}$ for the blended amines studied in this work is not more than 4 times smaller than that of MDEA. A lower value can be considered unlikely since the experimentally determined $D_{amine,\ solution}$ for other amines like MEA and diethanolamine (DEA), with similar concentration/viscosities, varies less than two times the value of the $D_{MDEA,\ solution}$ (Snijder et al., 1993). Overall, it can be concluded

that the kinetic experiments in this work were carried out under pseudo-first order conditions.

6.3. Viscosity

The viscosity of the blended amines is listed in Table 3 and presented in Fig. 5 along with viscosity data for DEEA/MAPA solutions reported by Monteiro et al. (2015). The viscosity decreased with increasing temperature and increased with increasing concentration of the tertiary amine blended with MAPA. The blended amines with equal molarity showed similar viscosities. The viscosity indirectly affects the CO_2 diffusivity coefficient, in which a decrease in the solution viscosity leads to an increase in the CO_2 diffusivity coefficient (Bernhardsen et al., 2019a).

6.4. Density

The density of the blended amines is tabulated in Table 4 and presented in Fig. 6 along with density data for DEEA/MAPA solutions reported by Monteiro et al. (2015). The density decreased with increasing temperature and decreased with increasing concentration of the tertiary amine blended with MAPA. For the blended amines with equal molarity, the density for 1-(2HE)PRLD blended with MAPA was the highest. The density of 3DMA1P/MAPA solutions was slightly lower than that of the DEEA/MAPA solutions.

6.5. N_2O solubility

The measured Henry's law constant for N_2O into the blended amines is listed in Table 5 and shown in Fig. 7, along with data for 1 M MAPA reported by Monteiro et al. (2014), 30 wt% MEA reported by Bernhardsen et al. (2019a) and DEEA/MAPA systems reported by Monteiro et al. (2015). In addition, for comparison reasons a second data set for 3 M DEEA + 1 M MAPA was generated in this work. This data set was found to be comparable to the data from Monteiro et al. (2015).

Fig. 7 shows that the N_2O solubility (inverse of Henry's law constant) is dependent on the temperature, the solvent concentration and the molecular structure of the tertiary amine blended with MAPA. For all the solvent systems, the solubility of N_2O decreased with increasing temperature. However, compared to 1 M MAPA, the Henry's law constant for N_2O into the blended amines was less sensitive to a change in temperature. At 25 °C, the Henry's law constant for N_2O into the 2 M DEEA + 1 M MAPA solution was higher than for the 1 M MAPA solution while, at a temperature higher than 55 °C, all the blended amines obtained a lower Henry's law constant.

Further, the solubility of N_2O increased with increasing concentration of the tertiary amine blended with 1 M MAPA. Interestingly, among the blended amines with equal molarity, the N_2O solubility was about the same into the 3DMA1P/MAPA and 1-(2HE)PRLD/MAPA solutions, while it was notably higher in blends of DEEA/MAPA. For instance, at 50 °C, the Henry's law constant for N_2O in the 3 M DEEA + 1 M MAPA solution was between 20 and 32 % lower than the other blended amines with the same molarity.

It is reported that the solubility of gaseous molecules depend on how the molecules arrange themselves in the liquid (Hamza et al., 1981; Li and Mather, 1994; Wang et al., 1992). Hamza et al. (1981) reported that aliphatic compounds could accommodate more gaseous molecules than cyclic compounds due to larger free space left available in the liquid, and this explain the higher solubility of N_2O

Table 3
Viscosity data for aqueous solutions of 3DMA1P and 1-(2HE)PRLD blended with MAPA, mPa·s.

T (°C)	2 M 3DMA1P + 1 M MAPA	3 M 3DMA1P + 1 M MAPA	4 M 3DMA1P + 1 M MAPA	3 M 1-(2HE)PRLD + 1 M MAPA
25	4.13	7.05	11.60	7.29
30	3.41	5.74	8.92	5.77
40	2.41	3.75	5.68	3.87
50	1.80	2.70	3.90	2.81
60	1.39	1.99	2.80	2.09
70	1.11	1.54	2.10	1.63
80	0.91	1.23	1.64	1.31

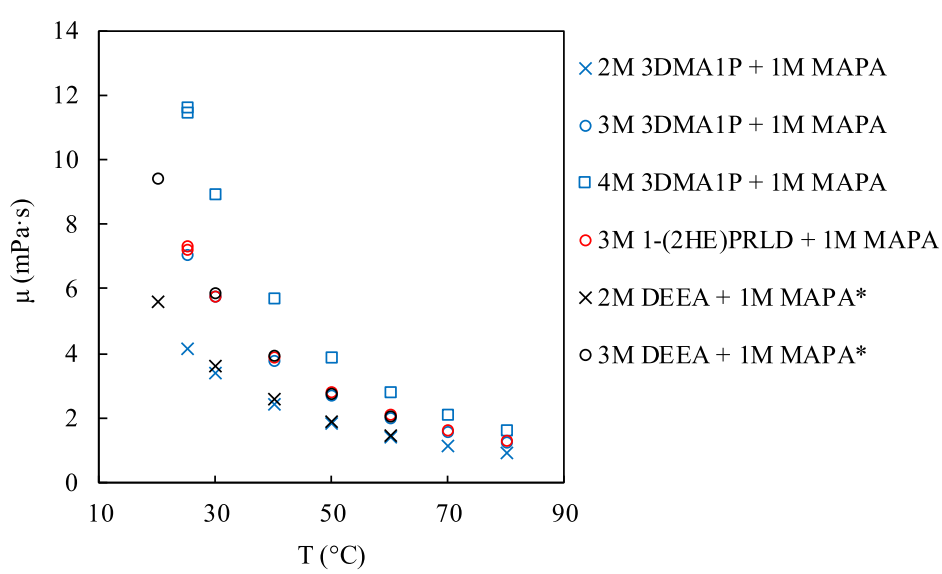

Fig. 5. Viscosity (μ) of MAPA promoted tertiary amines. *Monteiro et al. (2015).

Table 4
Density data for aqueous solutions of 3DMA1P and 1-(2HE)PRLD blended with MAPA, g cm^{-3}.

T (°C)	2 M 3DMA1P + 1 M MAPA	3 M 3DMA1P + 1 M MAPA	4 M 3DMA1P + 1 M MAPA	3 M 1-(2HE)PRLD + 1 M MAPA
25	0.9845	0.9789	0.9693	1.0073
30	0.9818	0.9755	0.9658	1.0038
40	0.9755	0.9681	0.9577	0.9962
50	0.9690	0.9607	0.9496	0.9888
60	0.9619	0.9528	0.9412	0.9808
70	0.9547	0.9449	0.9326	0.9728
80	0.9469	0.9365	0.9233	0.9643

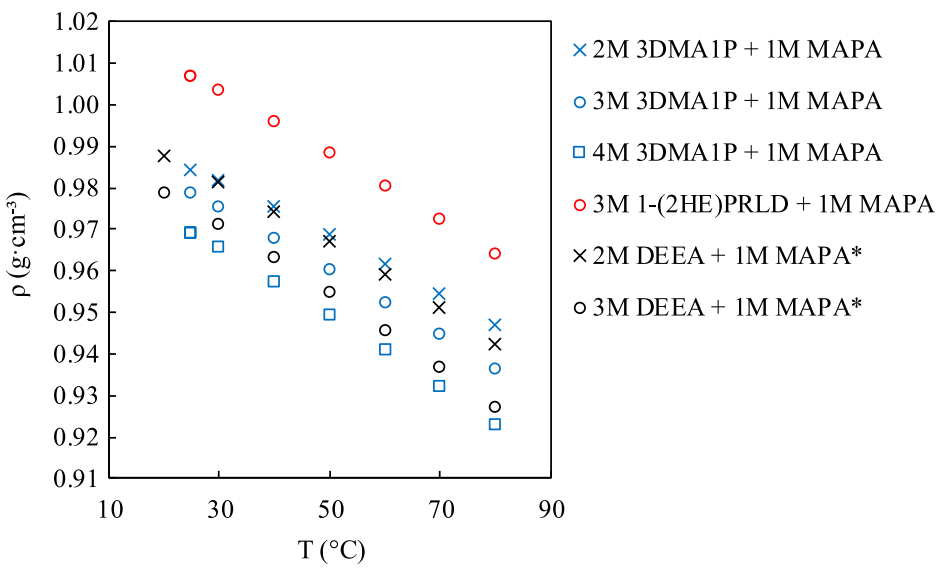

Fig. 6. Density (ρ) of MAPA promoted tertiary amines. *Monteiro et al. (2015).

Table 5
Measured Henry's law constant for N_2O in aqueous solutions of 3DMA1P and 1-(2HE)PRLD blended with MAPA. kPa m^3 mol^{-1}.

T (°C)	2 M 3DMA1P + 1 M MAPA	3 M 3DMA1P + 1 M MAPA	4 M 3DMA1P + 1 M MAPA	3 M 1-(2HE)PRLD + 1 M MAPA
30	5.58	5.48	4.69	5.15
30	5.59	5.45	4.66	5.14
40	6.39	6.02	5.10	5.68
40	6.42	6.01	5.06	5.66
50	7.14	6.51	5.47	6.18
50	7.17	6.51	5.43	6.17
60	7.85	6.96	5.80	6.63
60	7.87	6.99	5.75	6.64
70	8.56	7.35	6.12	7.05
70	8.48	7.39	6.07	7.07
80	9.07	7.66	6.41	7.45
80	9.09	7.79	6.31	7.41
90	9.43	8.00	6.68	7.81
90	9.62	8.14	6.57	7.76

in the DEEA/MAPA blends as compared to 3DMA1P/MAPA. The reason why, in the blend with MAPA, 3DMA1P obtained a solubility more similar to the cyclic 1-(2HE)PRLD than DEEA might have been due to the formation of intramolecular interactions, e.g. hydrogen bonds between the nitrogen and the hydrogen atom. From Fig. 8 it can be seen that these interactions in 3DMA1P lead to a 6-membered ring which is more stable than a 5-membered ring that occurs in DEEA.

6.6. Mass transfer and kinetics of MAPA promoted tertiary amines

The overall mass transfer coefficient (K_{ov}) combines the contribution of diffusion, physical absorption and chemical reaction to the mass transfer, and thereby represent the actual observed CO_2 absorption rate into the solvent. The K_{ov} values for the blended amines are presented in Fig. 9 along with the DEEA/MAPA solutions reported by Monteiro et al. (2015), 1 M MAPA reported by Monteiro et al. (2014) and 30 wt% MEA reported by Bernhardsen et al. (2019a). From the figure, it can be seen that the K_{ov} increased with increasing temperature. This is probably due to increasing reaction kinetics and increasing CO_2 diffusivity coefficient (Section 6.3) which follows at higher temperatures.

Further, the blended amines obtained quite similar K_{ov} values throughout the temperature range. This even though the solubility of N_2O in DEEA/MAPA solutions was higher than in the other blended amines (Section 6.5), and the solvent's viscosity increased with increasing solvent concentration which led to a decrease in CO_2 diffusivity (Section 6.3). Thus, competing effects between reac-

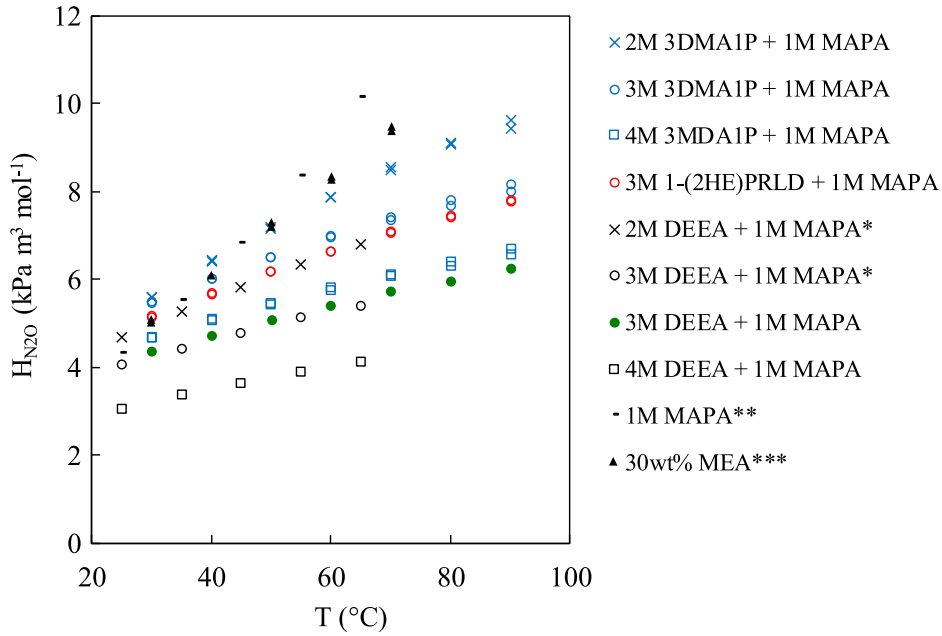

Fig. 7. The Henry's law constant for N_2O in amine solutions. *Monteiro et al. (2015); **Monteiro et al. (2014); ***Bernhardsen et al. (2019a).

tion kinetics, diffusivity and solubility likely played a key role in determining the K_{ov}.

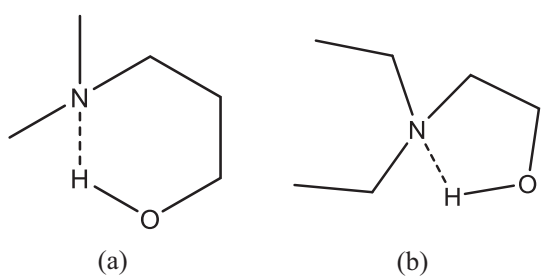

Fig. 8. The possible intramolecular interactions between the nitrogen and the hydrogen atom in (a) 3DMA1P and (b) DEEA.

Moreover, the blended amines obtained comparable K_{ov} values to that of 1 M MAPA. Compared to 30 wt% MEA, the K_{ov} values were in the same order of magnitude, but around 1.4 times higher.

A parameter influencing the mass transfer is the gas film resistance ($1/k_g$). The parameter is typically found to be important in regions where the CO_2 loading is low. In a conventional absorption process, this is located in the top and in the bottom of the absorption and desorption column, respectively (Cullinane and Rochelle, 2006). Fig. 10 shows the percentage contribution of the gas film resistance to the overall resistance (i.e. K_{ov}/k_g) as a function of temperature. The contribution of the gas film resistance increased with increasing temperature and, at 62.6 °C, the gas film resistance contributed up to 41% of the overall resistance. Aronu et al. (2011) obtained a similar trend as faster reaction kinetics lead to a higher contribution of the gas film resistance to the overall resistance. Consequently, the unloaded amine solutions studied in this work

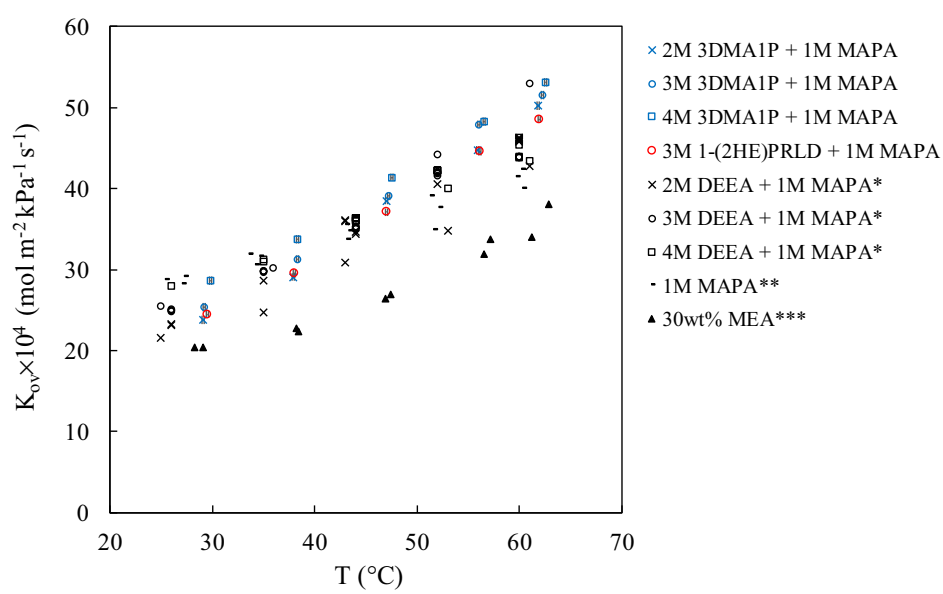

Fig. 9. Overall mass transfer coefficient (K_{ov}) as a function of temperature. *Monteiro et al. (2015), **Monteiro et al. (2014) ***Bernhardsen et al. (2019a).

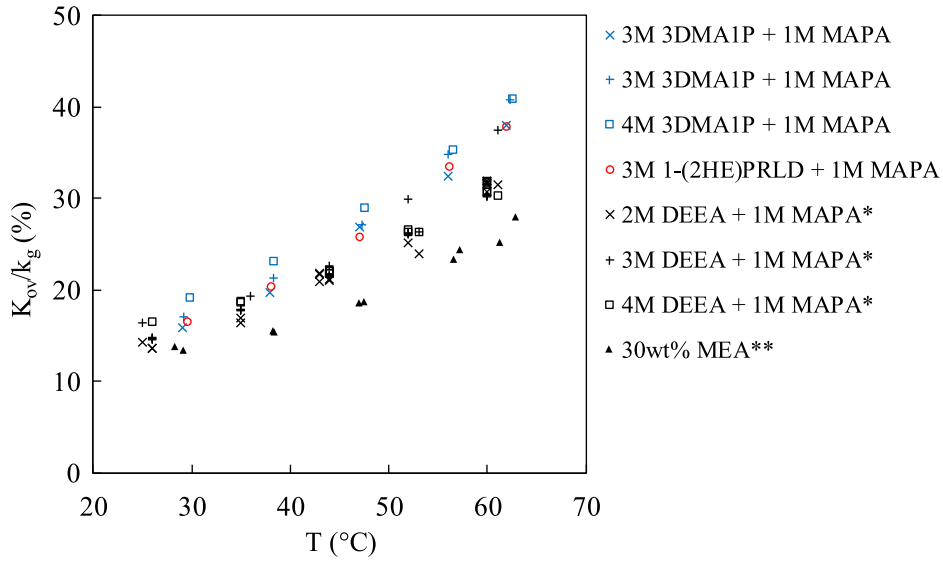

Fig. 10. Contribution of the gas film resistance (k_g) to the overall mass transfer (K_{ov}). *Monteiro et al. (2015), **Bernhardsen et al. (2019a).

were mainly kinetically controlled, but the influence of the gas film resistance to the overall resistance increased with increasing temperature. The DEEA/MAPA solvent systems reported by Monteiro et al. (2015) showed lower K_{ov}/k_g values than the other blended amines, but still higher than that of 30 wt% MEA reported by Bernhardsen et al. (2019a).

The pseudo-first order kinetic constant (k_{obs}) for the blended amines was calculated as given in Eq. (12) using experimental data for viscosity, density and Henry's law constant. Interpolated values were used at temperatures different from those measured, and the data used for the calculation are summarised in Appendix B. Fig. 11 presents the k_{obs} as a function of temperature for the blended amines studied in this work along with the DEEA/MAPA solutions reported by Monteiro et al. (2015), 1 M MAPA reported by Monteiro et al. (2014) and 30 wt% MEA reported by Bernhardsen et al. (2019a). The figure shows that the k_{obs} depend on the temperature, the molecular structure of the tertiary amine and the solution concentration. The k_{obs} increased with increasing temperature, and for the blended amines with equal molarity and viscosity, the order of increasing k_{obs} was DEEA/MAPA < 1-(2HE)PRLD/MAPA < 3DMA1P/MAPA at temperatures higher than 30 °C. This, difference was obtained despite the small difference detected in the pH value of the unloaded solutions. The pH of DEEA, 3DMA1P and 1-(2HE)PRLD blended with MAPA at 25 °C was measured to be 12.95, 12.96 and 12.81, respectively (repeatability ± 0.1 pH). Nevertheless, although the DEEA/MAPA solutions obtained lower k_{obs} values, the slower kinetic was compensated by the higher CO_2 solubility (smaller Henry's law constant) which resulted into comparable K_{ov} values as discussed above (Fig. 9).

Further, when looking at the different 3DMA1P/MAPA solutions presented in Fig. 11, it can be seen that the k_{obs} values increase with increasing concentration of 3DMA1P until a temperature of 47 °C. At higher temperatures, the 3 M 3DMA1P + 1 M MAPA solution shows higher k_{obs} values than the most concentrated solution. However, as above, the advantage of higher k_{obs} values is small when one considers the comparable K_{ov} values. The comparable K_{ov} values, when increasing the amine concentration, was due to the combination of increased viscosity (decreased CO_2 diffusivity), increased physical

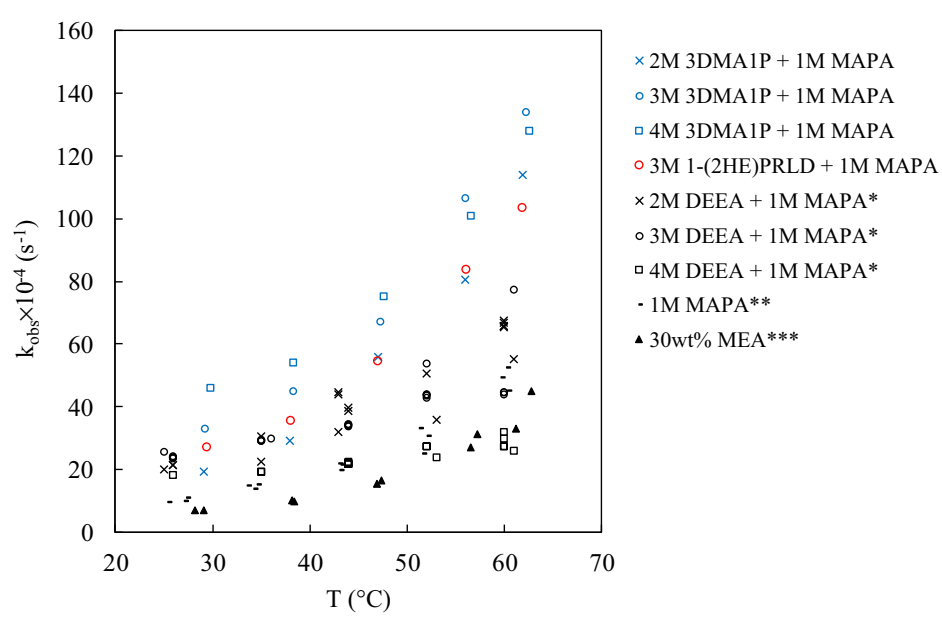

Fig. 11. Pseudo-first order kinetic constant (k_{obs}) as a function of temperature. *Monteiro et al. (2015); **Monteiro et al. (2014);***Bernhardsen et al. (2019a).

solubility and increased reaction kinetics. Thus, the results illustrate that k_{obs} alone cannot be used to identify fast CO_2 absorbents as the absorption rate also depends on the diffusivity and physical solubility. This is also clear when looking at the k_{obs} and K_{ov} values for 1 M MAPA and 30 wt% MEA. The values for k_{obs} were lower than the solvents studied in this work while the K_{ov} was comparable mainly due to their low solvents viscosity (high CO_2 diffusivity) (Amundsen et al., 2009; Monteiro et al., 2014).

6.7. Modelling of the pseudo-first order kinetic constant (k_{obs})

The pseudo-first order kinetic constant (k_{obs}) was modelled using the experssion for k_{obs} derived from the direct mechanism given in Eq. (7) where MAPA, H_2O, and the tertiary amine are considered possible proton receivers. As seen from the equation, it was assumed additive kinetic effects of MAPA, H_2O and the tertiary amine on the k_{obs}. Similar to the work by Monteiro et al. (2015), the kinetic constants for MAPA, k_{MAPA}, and H_2O, k_{H_2O}, respectively, were retrieved from Monteiro et al. (2014). Then, with known concentrations for each component in the solution and the calculated k_{obs} values (Appendix B), the kinetic constant for 3DMA1P (k_{3DMA1P}) and 1-(2HE)PRLD ($k_{1\text{-}(2HE)PRLD}$), respectively, was determined (Eqs. (28) and (29)). It should be noted that the expression for k_{3DMA1P} (Eq. (28)), covers three solvent concentrations, while the expression for $k_{1\text{-}(2HE)PRLD}$ (Eq. (29)), is only valid for one solvent concentration.

$$k_{3DMA1P} = 7.799 \times 10^4 \exp\left(\frac{-4247}{T}\right) \tag{28}$$

$$k_{1\text{-}(2HE)PRLD} = 1.432 \times 10^5 \exp\left(\frac{-4522}{T}\right) \tag{29}$$

Fig. 12 shows that the modelled k_{obs} adequate correlate to the k_{obs} calculated from Eq. (7). The AARD for the 3DMA1P/MAPA and 1-(2HE)PRLD/MAPA solutions was 11.1% and 3.3%, respectively, in which the higher AARD for the 3DMA1P/MAPA solution was due to less accurate predictions of the k_{obs} at high temperatures. This was probably because Eq. (28) covered three solvent concentrations. The figure further shows that the effect of H_2O on the k_{obs} is very small even though the concentration of H_2O in the solution is 6 to 20 times higher than the concentration of the amine.

The terms $k_{3DMA1P}c_{3DMA1P}c_{MAPA}$ and $k_{1\text{-}(2HE)PRLD}c_{1\text{-}(2HE)PRLD}c_{MAPA}$, given in Eq. (7), represent the effect of the tertiary amine as a proton receiver for the MAPA-CO_2 reaction (Eq. (1)) on k_{obs}. In this work, these terms were found to contribute between 54 and 70% and 56–59%, respectively, to the k_{obs}. Monteiro et al. (2015) reported that the term $k_{DEEA}c_{DEEA}c_{MAPA}$, for DEEA blended with 1 M MAPA, contributed between 52 and 95 % of the total k_{obs}.

Further, in the temperature range of 38–47 °C, the contribution of $k_{3DMA1P}c_{3DMA1P}c_{MAPA}$ to k_{obs} increased from 54 to 70% with an increase in 3DMA1P concentration (Fig. 12a-c). A similar observation was also reported in Monteiro et al. (2015) for DEEA blended with 2 M MAPA. Since the pKa value of 3DMA1P (pKa = 9.48) and DEEA (pKa = 9.84) is larger than pKa2 (8.6) of MAPA, it can increase the availability of MAPA to form carbamate (Bernhardsen et al., 2018) as less MAPA will be protonated. Moreover, 3DMA1P and DEEA, in the protonated form, can act as a counter-ion of MAPA carbamates (Eq. (1)) (Perinu et al., 2018). Thus, when the concentration of 3DMA1P and DEEA increases, there might be less protonated MAPA, and then, more amino nitrogen available to form MAPA carbamate, leading to faster reaction kinetics.

At last, the results and the comparison with literature data presented in this work indicates that when it comes to the kinetics, the studied solvent systems are promising solvents for CO_2 capture

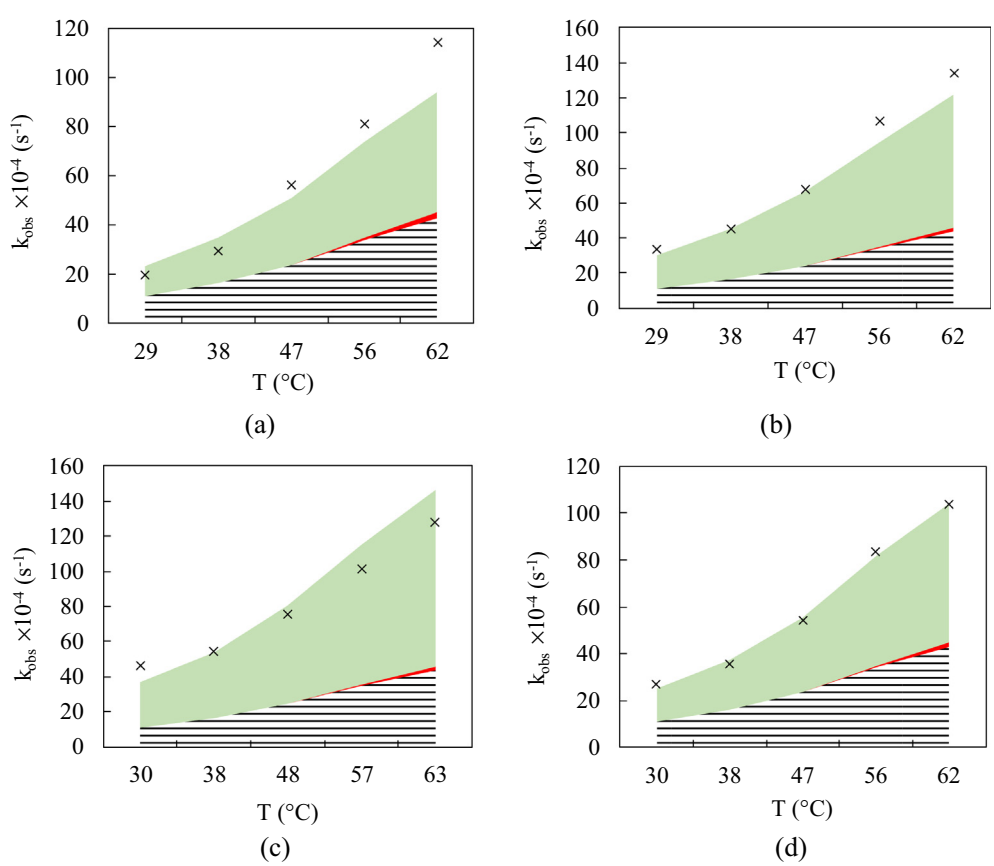

Fig. 12. Contribution of the observed pseudo-first order kinetic constant (k_{obs}). (a) 2 M 3MDA1P + 1 M MAPA; (b) 3 M 3DMA1P + 1 M MAPA; (c) 4 M 3DMA1P + 1 M MAPA; (d) 3 M 1-(2HE)PRLD + 1 M MAPA; green, tertiary amine; red, H2O; =, MAPA, × experimental k_{obs}.

by means of chemical absorption with a performance similar to that of DEEA/MAPA.

7. Conclusions

The initial absorption kinetics of CO_2 into unloaded aqueous solutions of 3DMA1P and 1-(2HE)PRLD blended with 1 M MAPA was studied using a string of discs contactor. The experiments were conducted in the temperature range of 29–63 °C and carried out under pseudo-first order conditions. In addition, viscosity, density and N_2O solubility were measured. The results obtained in this work were compared to DEEA/MAPA solutions.

The blended amines studied in this work, as well as DEEA/MAPA solutions, showed similar values for the overall mass transfer coefficient. This was explained by the competing effects between diffusivity, solubility and reaction kinetics. The solubility of N_2O was higher in DEEA/MAPA than in the other blended amines, while the k_{obs} was higher for 3DMA1P/MAPA and 1-(2HE)PRLD/MAPA solutions than that of DEEA/MAPA. In addition, the viscosity was found to increase with increasing concentration of the tertiary amine in the blend with MAPA and, at equal molarity, the viscosity of the blended amine solvents was similar. The obtained overall mass transfer coefficients for the blended amines were comparable to 1 M MAPA and around 1.4 times higher than that of 30 wt% MEA. Further, a correlation for k_{obs} was represented using the direct mechanism with reasonable accuracy. The contribution of the tertiary amine as a proton receiver for the MAPA-CO_2 reaction accounted for 54–70% of the pseudo-first order kinetic constant.

Declaration of Competing Interest

None.

Acknowledgement

The work has been a part of the Low energy Penalty Solvents (LEPS) project with grant number 243620 under the CLIMIT programme. The authors would like to thank the Research Council of Norway for financial support. Cristina Perinu is acknowledged for participating in discussions as well as running some of the viscosity and density measurements.

Appendix A

See Tables A1 and A2.

Table A1
Measured Henry's constant for N_2O in water.

T (°C)	$H_{N2O,water}$ (kPa m^3 mol^{-1})
30.0	4.72
30.0	4.76
40.0	5.97
40.0	6.03
50.0	7.28
50.0	7.34
60.0	8.63
60.0	8.84
70.0	10.13
70.0	10.05
80.1	11.44
80.1	11.35
90.0	12.81
90.0	12.83

Table A2
Measured Henry's law constant for CO_2 in water.

T (°C)	$H_{CO2,water}$ (kPa m^3 mol^{-1})
30.0	3.42
30.0	3.43
40.0	4.29
40.0	4.30
50.0	5.20
50.0	5.21
60.0	6.12
60.0	6.14
80.1	8.01
80.0	7.95
90.0	8.85

Appendix B

See Table B1.

Table B1
Experimental and calculated results for the blended amines 3DMA1P/MAPA and 1-(2HE)PRLD/MAPA using the string of discs contactor.

Experiment	T	ρ	μ	H_{CO2}	$p_{solution}$	$D_{CO_2,solution} \times 10^{10}$	$N_{CO2} \times 10^4$	LMP_{CO2}	$K_{ov} \times 10^4$	$k_g \times 10^2$	$k_l^o \times 10^5$	$k_{obs} \times 10^{-4}$	Ha	α*
	°C	kg m^{-3}	mPa s	kPa m^3 mol^{-1}	kPa	m^2 s^{-1}	mol m^{-2} s^{-1}	kPa	mol m^{-2} kPa^{-1} s^{-1}	mol m^{-2} kPa^{-1} s^{-1}	m s^{-1}	s^{-1}		
2 M (21.0 wt%) 3DMA1P, 1 M (9.0 wt%) MAPA	29.1	983	3.53	3.98	3.8	6.57	5.69	0.239	23.80	1.50	2.84	19.34	397	0.008
	37.9	976	2.58	4.45	6.2	8.93	6.27	0.216	29.09	1.48	3.85	29.06	419	0.009
	47.0	970	1.95	4.89	10.0	11.84	7.11	0.185	38.49	1.43	5.09	55.92	505	0.013
	56.0	964	1.54	5.30	15.5	15.23	8.94	0.200	44.71	1.38	6.49	80.70	540	0.020
	61.9	960	1.34	5.56	20.4	17.78	9.94	0.198	50.22	1.32	7.47	114.02	603	0.025
3 M (31.7 wt%) 3DMA1P, 1 M (9.0 wt%) MAPA	29.2	976	5.90	3.93	3.7	4.36	5.68	0.224	25.36	1.49	1.78	33.06	675	0.005
	38.3	969	4.05	4.22	6.1	6.23	6.43	0.206	31.30	1.47	2.56	45.13	654	0.006
	47.3	962	2.92	4.49	9.7	8.61	7.33	0.188	39.06	1.44	3.53	67.20	681	0.009
	56.0	956	2.22	4.74	15.0	11.37	9.21	0.192	47.91	1.38	4.63	106.61	752	0.014
	62.3	951	1.88	4.91	20.0	13.60	10.00	0.194	51.51	1.26	5.52	133.91	773	0.019
4 M (42.7 wt%) 3DMA1P, 1 M (9.1 wt%) MAPA	29.8	966	9.03	3.38	3.6	3.11	6.21	0.217	28.63	1.50	1.21	45.98	991	0.004
	38.3	959	6.07	3.57	5.8	4.51	7.12	0.211	33.72	1.46	1.77	54.31	886	0.006
	47.6	951	4.23	3.77	9.4	6.41	8.00	0.193	41.36	1.43	2.51	75.18	874	0.008
	56.6	944	3.15	3.95	14.5	8.64	9.08	0.188	48.25	1.36	3.36	100.96	878	0.011
	62.6	939	2.62	4.07	19.2	10.45	10.14	0.191	53.09	1.30	4.05	127.95	904	0.014
3 M 1-(2HE)PRLD (34.4 wt%), 1 M MAPA (8.8 wt%)	29.5	1004	5.90	3.70	3.7	4.37	6.00	0.245	24.49	1.48	1.81	27.02	599	0.005
	38.0	997	4.16	3.97	5.9	6.09	5.96	0.202	29.56	1.45	2.54	35.67	580	0.007
	47.0	990	3.06	4.25	9.4	8.28	6.87	0.185	37.07	1.43	3.44	54.41	618	0.010
	56.2	983	2.35	4.51	14.8	10.90	7.78	0.175	44.56	1.33	4.48	83.76	675	0.013
	61.9	979	2.01	4.67	19.3	12.87	9.16	0.189	48.56	1.28	5.25	103.53	695	0.016

* CO_2 loading (mol_{CO2}/mol_{amine}) at the end of the experiment.

References

Amundsen, T.G., Øi, L.E., Eimer, D.A., 2009. Density and viscosity of monoethanolamine + water + carbon dioxide from (25 to 80) °C. J. Chem. Eng. Data 54, 3096–3100. https://doi.org/10.1021/je900188m.

Aronu, U.E., Hartono, A., Hoff, K.A., Svendsen, H.F., 2011. Kinetics of carbon dioxide absorption into aqueous amino acid salt: potassium salt of sarcosine solution. Ind. Eng. Chem. Res. 50, 10465–10475. https://doi.org/10.1021/ie200596y.

Bernhardsen, I.M., Ansaloni, L., Betten, H.K., Liyuan, D., Knuutila, H.K., 2019a. Effect of liquid viscosity on the performance of a non-porous membrane contactor for CO2 capture. Sep. Purif. Technol. 222, 188–201. https://doi.org/10.1016/j.seppur.2019.04.024.

Bernhardsen, I.M., Krokvik, I.R.T., Perinu, C., Pinto, D.D.D., Jens, K.J., Knuutila, H.K., 2018. Influence of pKa on solvent performance of MAPA promoted tertiary amines. Int. J. Greenhouse Gas Control 68, 68–76. https://doi.org/10.1016/j.ijggc.2017.11.005.

Bernhardsen, I.M., Trollebø, A.A., Perinu, C., Knuutila, H.K., 2019b. Vapour-liquid equilibrium study of tertiary amines, single and in blend with MAPA, for post combustion CO2 capture. J. Chem. Thermodyn. 138, 211–228. https://doi.org/10.1016/j.jct.2019.06.017.

Bingham, E.C., Jackson, R.F., 1917. Standard substances for the calibration of viscometers. J. Wash. Acad. Sci. 7, 53–55.

Blauwhoff, P.M.M., Versteeg, G.F., Van Swaaij, W.P.M., 1984. A study on the reaction between CO2 and alkanolamines in aqueous solutions. Chem. Eng. Sci. 39, 207–225. https://doi.org/10.1016/0009-2509(84)80021-4.

Brúder, P., Lauritsen, K.G., Mejdell, T., Svendsen, H.F., 2012. CO2 capture into aqueous solutions of 3-methylaminopropylamine activated dimethylmonoethanolamine. Chem. Eng. Sci. 75, 28–37. https://doi.org/10.1016/j.ces.2012.03.005.

Caplow, M., 1968. Kinetics of carbamate formation and breakdown. J. Am. Chem. Soc. 90, 6795–6803. https://doi.org/10.1021/ja01026a041.

Carroll, J.J., Slupsky, J.D., Mather, A.E., 1991. The solubility of carbon dioxide in water at low pressure. J. Phys. Chem. Ref. Data 20, 1201–1209. https://doi.org/10.1063/1.555900.

Clarke, J.K.A., 1964. Kinetics of absorption of cardon dioxide in monoethanolamine solutions at short contact times. Ind. Eng. Chem. Fundam. 3, 239–245. https://doi.org/10.1021/i160011a012.

Cullinane, J.T., Rochelle, G.T., 2006. Kinetics of carbon dioxide absorption into aqueous potassium carbonate and piperazine. Ind. Eng. Chem. Res. 45, 2531–2545. https://doi.org/10.1021/ie050230s.

Danckwerts, P.V., 1970. Gas-liquid Reactions. McGraw-Hill, New York.

Donaldson, T.L., Nguyen, Y.N., 1980. Carbon dioxide reaction kinetics and transport in aqueous amine membranes. Ind. Eng. Chem. Fundam. 19, 260–266. https://doi.org/10.1021/i160075a005.

Du, Y., Yuan, Y., Rochelle, G.T., 2016. Capacity and absorption rate of tertiary and hindered amines blended with piperazine for CO2 capture. Chem. Eng. Sci. 155, 397–404. https://doi.org/10.1016/j.ces.2016.08.017.

Evjen, S., Wanderley, R., Fiksdahl, A., Knuutila, H.K., 2019. Viscosity, density, and volatility of binary mixtures of imidazole, 2-methylimidazole, 2,4,5-trimethylimidazole, and 1,2,4,5-tetramethylimidazole with water. J. Chem. Eng. Data 64, 507–516. https://doi.org/10.1021/acs.jced.8b00674.

Gondal, S., Asif, N., Svendsen, H.F., Knuutila, H., 2015a. Density and N2O solubility of aqueous hydroxide and carbonate solutions in the temperature range from 25 to 80 °C. Chem. Eng. Sci. 122, 307–320. https://doi.org/10.1016/j.ces.2014.09.016.

Gondal, S., Asif, N., Svendsen, H.F., Knuutila, H., 2015b. Kinetics of the absorption of carbon dioxide into aqueous hydroxides of lithium, sodium and potassium and blends of hydroxides and carbonates. Chem. Eng. Sci. 123, 487–499. https://doi.org/10.1016/j.ces.2014.10.038.

Hamza, M.H.A., Serratrice, G., Stebe, M.J., Delpuech, J.J., 1981. Solute-solvent interactions in perfluorocarbon solutions of oxygen. An NMR study. J. Am. Chem. Soc. 103, 3733–3738. https://doi.org/10.1021/ja00403a020.

Hartono, A., da Silva, E.F., Svendsen, H.F., 2009. Kinetics of carbon dioxide absorption in aqueous solution of diethylenetriamine (DETA). Chem. Eng. Sci. 64, 3205–3213. https://doi.org/10.1016/j.ces.2009.04.018.

Hartono, A., Saleem, F., Arshad, M.W., Usman, M., Svendsen, H.F., 2013. Binary and ternary VLE of the 2-(diethylamino)-ethanol (DEEA)/3-(methylamino)-propylamine (MAPA)/water system. Chem. Eng. Sci. 101, 401–411. https://doi.org/10.1016/j.ces.2013.06.052.

Haubrock, J., Hogendoorn, J.A., Versteeg, G.F., 2007. The applicability of activities in kinetic expressions: A more fundamental approach to represent the kinetics of the system CO2–OH-–salt in terms of activities. Chem. Eng. Sci. 62, 5753–5769. https://doi.org/10.1016/j.ces.2007.06.018.

Idem, R., Wilson, M., Tontiwachwuthikul, P., Chakma, A., Veawab, A., Aroonwilas, A., Gelowitz, D., 2006. Pilot plant studies of the CO2 capture performance of aqueous MEA and mixed MEA/MDEA solvents at the university of regina CO2 capture technology development plant and the boundary dam CO2 capture demonstration plant. Ind. Eng. Chem. Res. 45, 2414–2420. https://doi.org/10.1021/ie050569e.

Li, L., Voice, A.K., Li, H., Namjoshi, O., Nguyen, T., Du, Y., Rochelle, G.T., 2013. Amine blends using concentrated piperazine. Energy Procedia 37, 353–369. https://doi.org/10.1016/j.egypro.2013.05.121.

Li, Y.-G., Mather, A.E., 1994. Correlation and prediction of the solubility of N2O in mixed solvents. Fluid Phase Equilib. 96, 119–142. https://doi.org/10.1016/0378-3812(94)80090-1.

Luo, X., Hartono, A., Hussain, S.F., Svendsen, H., 2015. Mass transfer and kinetics of carbon dioxide absorption into loaded aqueous monoethanolamine solutions. Chem. Eng. Sci. 123, 57–69. https://doi.org/10.1016/j.ces.2014.10.013.

Ma'mun, S., Dindore, V.Y., Svendsen, H.F., 2007. Kinetics of the reaction of carbon dioxide with aqueous solutions of 2-((2-aminoethyl)amino)ethanol. Ind. Eng. Chem. Res. 46, 385–394. https://doi.org/10.1021/ie060383v.

Ma'mun, S., Jakobsen, J.P., Svendsen, H.F., Juliussen, O., 2006. Experimental and modeling study of the solubility of carbon dioxide in aqueous 30 mass % 2-((2-aminoethyl)amino)ethanol solution. Ind. Eng. Chem. Res. 45, 2505–2512. https://doi.org/10.1021/ie0505209.

Monteiro, J.G.M.S., Hussain, S., Majeed, H., Mba, E.O., Hartono, A., Knuutila, H., Svendsen, H.F., 2014. Kinetics of CO2 absorption by aqueous 3-(methylamino) propylamine solutions: Experimental results and modeling. AIChE J. 60, 3792–3803. https://doi.org/10.1002/aic.14546.

Monteiro, J.G.M.S., Majeed, H., Knuutila, H., Svendsen, H.F., 2015. Kinetics of CO2 absorption in aqueous blends of N, N-diethylethanolamine (DEEA) and N-methyl-1,3-propane-diamine (MAPA). Chem. Eng. Sci. 129, 145–155. https://doi.org/10.1016/j.ces.2015.02.001.

Peng, D.-Y., Robinson, D.B., 1976. A new two-constant equation of state. Ind. Eng. Chem. Fundam. 15, 59–64. https://doi.org/10.1021/i160057a011.

Penttilä, A., Dell'Era, C., Uusi-Kyyny, P., Alopaeus, V., 2011. The Henry's law constant of N2O and CO2 in aqueous binary and ternary amine solutions (MEA, DEA, DIPA, MDEA, and AMP). Fluid Phase Equilib. 311, 59–66. https://doi.org/10.1016/j.fluid.2011.08.019.

Perinu, C., Bernhardsen, I.M., Pinto, D.D.D., H.K., K., Klaus, J.J., 2019. Aqueous MAPA, DEEA and their blend as CO2 absorbents: Interrelationship between NMR speciation, pH and heat of absorption data. Ind. Eng. Chem. Res. 58, 9781–9794. https://doi.org/10.1021/acs.iecr.9b01437.

Perinu, C., Bernhardsen, I.M., Pinto, D.D.D., Knuutila, H.K., Jens, K.-J., 2018. NMR speciation of aqueous MAPA, tertiary amines, and their blends in the presence of CO2: Influence of pKa and reaction mechanisms. Ind. Eng. Chem. Res. 57, 1337–1349. https://doi.org/10.1021/acs.iecr.7b03795.

Perry, R.H., Green, D.W., Maloney, J.O., 1997. Perry's Chemical Engineering Handbook. New York, McGraw-Hill.

Pinto, D.D.D., Knuutila, H., Fytianos, G., Haugen, G., Mejdell, T., Svendsen, H.F., 2014. CO2 post combustion capture with a phase change solvent. Pilot plant campaign. Int. J. Greenhouse Gas Control 31, 153–164. https://doi.org/10.1016/j.ijggc.2014.10.007.

Snijder, E.D., te Riele, M.J.M., Versteeg, G.F., van Swaaij, W.P.M., 1993. Diffusion coefficients of several aqueous alkanolamine solutions. J. Chem. Eng. Data 38, 475–480. https://doi.org/10.1021/je00011a037.

Sodiq, A., Hadri, N.E., Goetheer, E.L.V., Abu-Zahra, M.R.M., 2018. Chemical reaction kinetics measurements for single and blended amines for CO2 postcombustion capture applications. Int. J. Chem. Kinet. 50, 615–632. https://doi.org/10.1002/kin.21187.

Steeneveldt, R., Berger, B., Torp, T.A., 2006. CO2 capture and storage: closing the knowing-doing gap. Chem. Eng. Res. Des. 84, 739–763. https://doi.org/10.1205/cherd05049.

Versteeg, G.F., Van Swaaij, W.P.M., 1988. Solubility and diffusivity of acid gases (carbon dioxide, nitrous oxide) in aqueous alkanolamine solutions. J. Chem. Eng. Data 33, 29–34. https://doi.org/10.1021/je00051a011.

Wang, Y.W., Xu, S., Otto, F.D., Mather, A.E., 1992. Solubility of N2O in alkanolamines and in mixed solvents. Chem. Eng. J. 48, 31–40. https://doi.org/10.1016/0300-9467(92)85004-S.